Supplemental Document

Biomedical Optics EXPRESS

Unknown cell class distinction via neural network based scattering snapshot recognition: supplement

GAIA CIOFFI,[1,†] DAVID DANNHAUSER,[1,*,†] DOMENICO ROSSI,[2] PAOLO A. NETTI,[1,2] AND FILIPPO CAUSA[1]

[1] *Interdisciplinary Research Centre on Biomaterials (CRIB) and Dipartimento di Ingegneria Chimica, dei Materiali e della Produzione Industriale, Università degli Studi di Napoli "Federico II", Piazzale Tecchio 80, 80125 Naples, Italy*
[2] *Center for Advanced Biomaterials for Healthcare@CRIB, Istituto Italiano di Tecnologia, Largo Barsanti e Matteucci 53, 80125 Naples, Italy*
[†] *These authors contributed equally to this work*
[*] *david.dannhauser@unina.it*

This supplement published with Optica Publishing Group on 6 September 2023 by The Authors under the terms of the Creative Commons Attribution 4.0 License in the format provided by the authors and unedited. Further distribution of this work must maintain attribution to the author(s) and the published article's title, journal citation, and DOI.

Supplement DOI: https://doi.org/10.6084/m9.figshare.23813541

Parent Article DOI: https://doi.org/10.1364/BOE.492028

Electronic Supplementary Information:

Unknown cell class distinction via neural network based scattering snapshot recognition

GAIA CIOFFI,[1,†] DAVID DANNHAUSER,[1,†,*] DOMENICO ROSSI,[2] PAOLO A. NETTI[1,2] AND FILIPPO CAUSA,[1]

[1]*Interdisciplinary Research Centre on Biomaterials (CRIB) and Dipartimento di Ingegneria Chimica, dei Materiali e della Produzione Industriale, Università degli Studi di Napoli "Federico II", Piazzale Tecchio 80, 80125 Naples, Italy*
[2] *Center for Advanced Biomaterials for Healthcare@CRIB, Istituto Italiano di Tecnologia, Largo Barsanti e Matteucci 53, 80125 Naples, Italy*
†These authors contributed equally to this work
**david.dannhauser@unina.it*

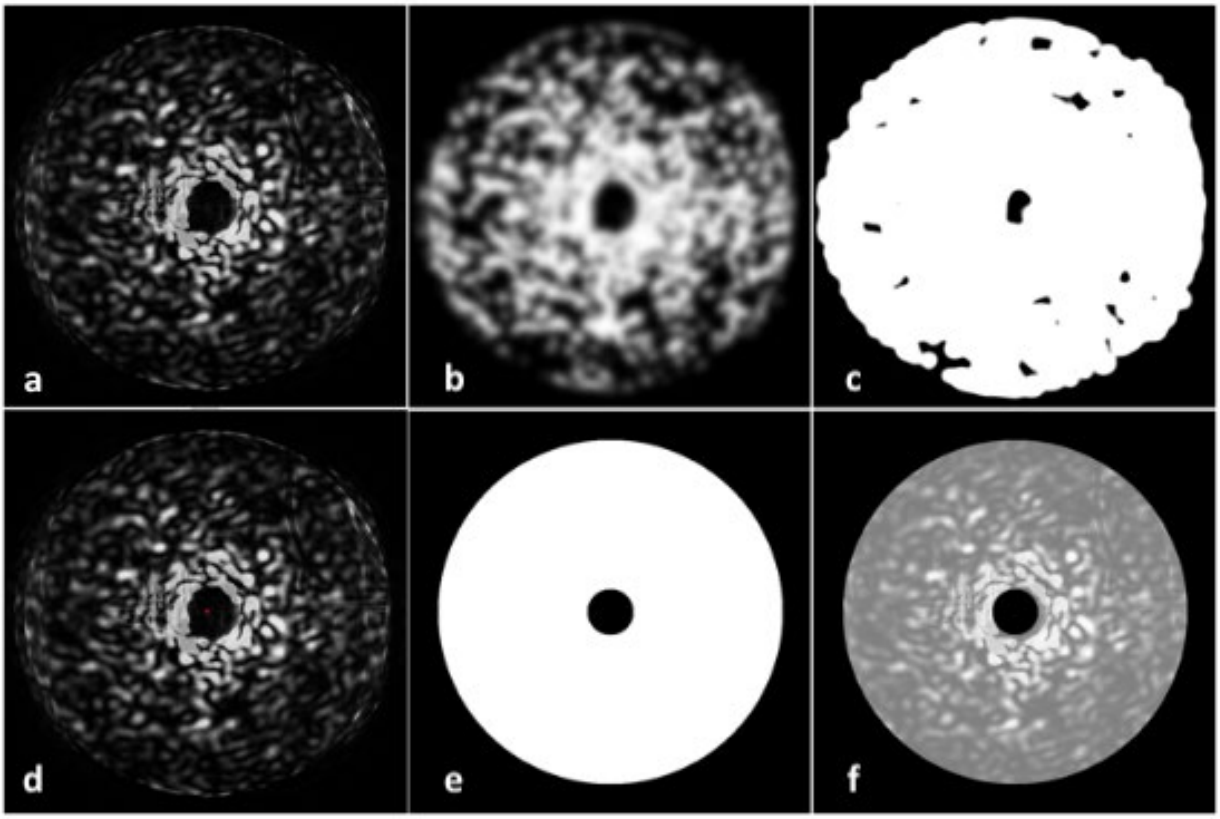

Fig. S1: Illustrative scattering snapshots pre-processing: (a) on the raw scattering snapshot, (b) a 2D gaussian low-pass filter (size 15x15 pixel and standard deviation of 6) was iteratively applied four times, followed by a spot-enhancement using a low-light image enhancement based on inversion of low-light image (build in MATLAB function called imcomplement), applying a haze removal algorithm (build in MATLAB function called imreducehaze) and an inversion of the enhanced snapshot image (build in MATLAB function called imcomplement). Note that haze thickness at each pixel and the estimated atmospheric light were not used for the snapshot pre-processing. Then, snapshot intensity values were mapped on new values before a global threshold. All these steps are done to merge the separated snapshot components in a unique binary mask (c), to finally perform a segmentation on the raw scattering snapshot. Subsequently, a centroid detection function returns the 0° coordinate of the scattering snapshot (d). The centroid value was used as the centre for a donut mask (e) used to perform segmentation on the raw snapshot (f).

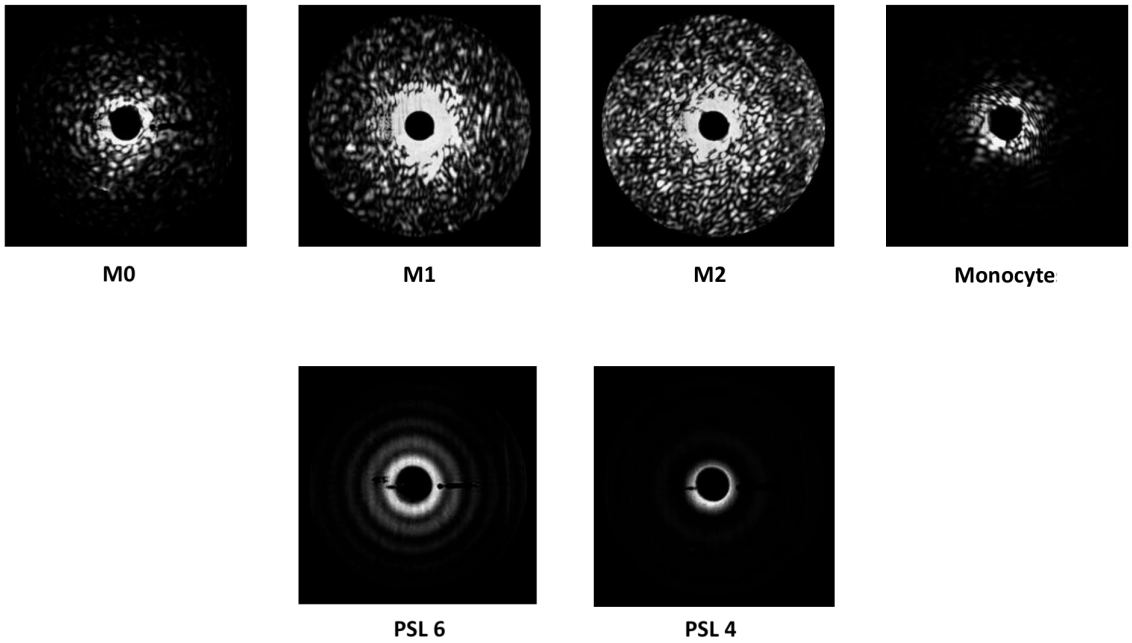

Fig. S2: M0-, M1-, M2- macrophages and Monocytes scattering snapshots shown respectively in the first row were calibrated and tested with polystyrene beads (PSL) of 6 and 4 µm scattering snapshots shown in the second row.

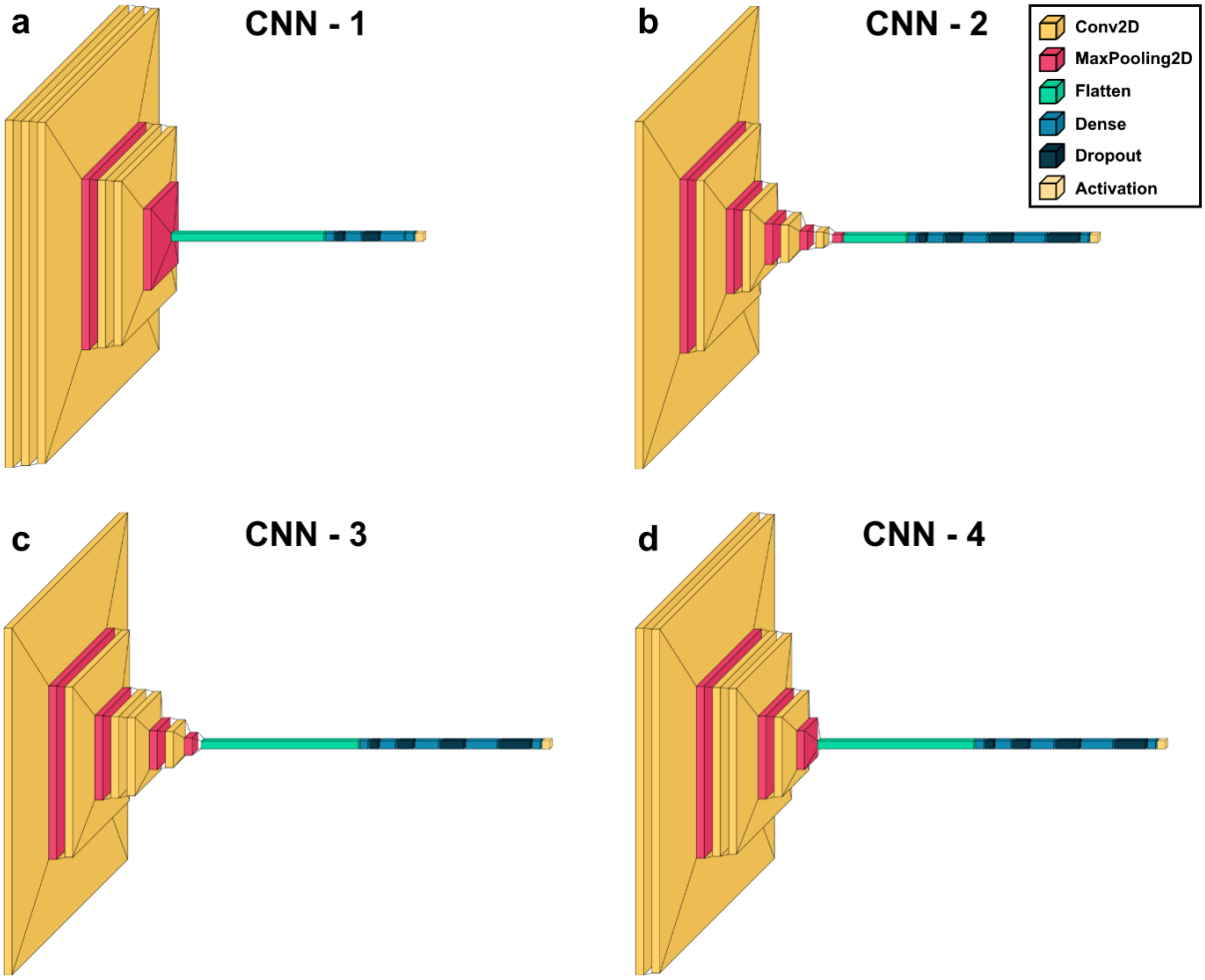

Fig. S3: Illustration of CNN architecture development. Model accuracy and detection rate were tested for M0, M1, M2-macrophages and monocytes using (a) 35.0x10^6, (b) 1.3x10^6, (c) 2.5x10^6 and (d) 9.0x10^6 trainable parameters.

Table S1. Detailed parameter list for the CNN architectures of Fig. S3. We set a kernel size of (3x3), a dropout percentage of 0.2, a batch size equal to 32 and a SoftMax activation function. The Adam optimizer algorithm has been used as optimization function, with a learning rate equal to 0.0001 for CNN - 1 and CNN - 3 and equal to 0.0005 for CNN - 2 and CNN - 4.

CNN - 1

Layer type	Output shape	Number of parameters
Convolution	(222x222x16)	160
Convolution	(220x220x32)	4640
Convolution	(218x218x48)	13872
Max Pooling	(109x109x48)	0
Convolution	(107x107x64)	27712
Convolution	(105x105x64)	36928
Max Pooling	(52x52x64)	0
Flatten	173056	0
Dense	200	34611400
Dropout	200	0
Dense	400	80400
Dropout	400	0
Dense	600	240600
Dense	4	2404
Activation	4	0

CNN - 2

Layer type	Output shape	Number of parameters
Convolution	(222x222x64)	640
Max Pooling	(111x111x64)	0
Convolution	(109x109x64)	36928
Max Pooling	(54x54x64)	0
Convolution	(52x52x64)	36928
Max Pooling	(26x26x64)	0
Convolution	(24x24x64)	36928
Max Pooling	(12x12x64)	0
Convolution	(10x10x64)	36928
Max Pooling	(5x5x64)	0
Flatten	1600	0
Dense	200	320200
Dropout	200	0
Dense	400	80400
Dropout	400	0
Dense	600	240600
Dropout	600	0
Dense	800	480800
Dropout	800	0
Dense	4	3204
Activation	4	0

CNN - 3

Layer type	Output shape	Number of parameters
Convolution	(222x222x64)	640
Max Pooling	(111x111x64)	0
Convolution	(109x109x64)	36928
Max Pooling	(54x54x64)	0
Convolution	(52x52x64)	36928
Convolution	(50x50x64)	36928
Max Pooling	(25x25x64)	0
Convolution	(23x23x64)	36928
Max Pooling	(11x11x64)	0
Flatten	7744	0
Dense	200	1549000
Dropout	200	0
Dense	400	80400
Dropout	400	0
Dense	600	240600
Dropout	600	0
Dense	800	480800
Dropout	800	0
Dense	4	3204
Activation	4	0

CNN - 4 Layer type	Output shape	Number of parameters
Convolution	(222x222x64)	640
Convolution	(220x220x64)	36928
Max Pooling	(110x110x64)	0
Convolution	(108x108x64)	36928
Convolution	(106x106x64)	36928
Max Pooling	(53x53x64)	0
Convolution	(51x51x64)	36928
Max Pooling	(25x25x64)	0
Flatten	40000	0
Dense	200	8000200
Dropout	200	0
Dense	400	80400
Dropout	400	0
Dense	600	240600
Dropout	600	0
Dense	800	480800
Dropout	800	0
Dense	4	3204
Activation	4	0

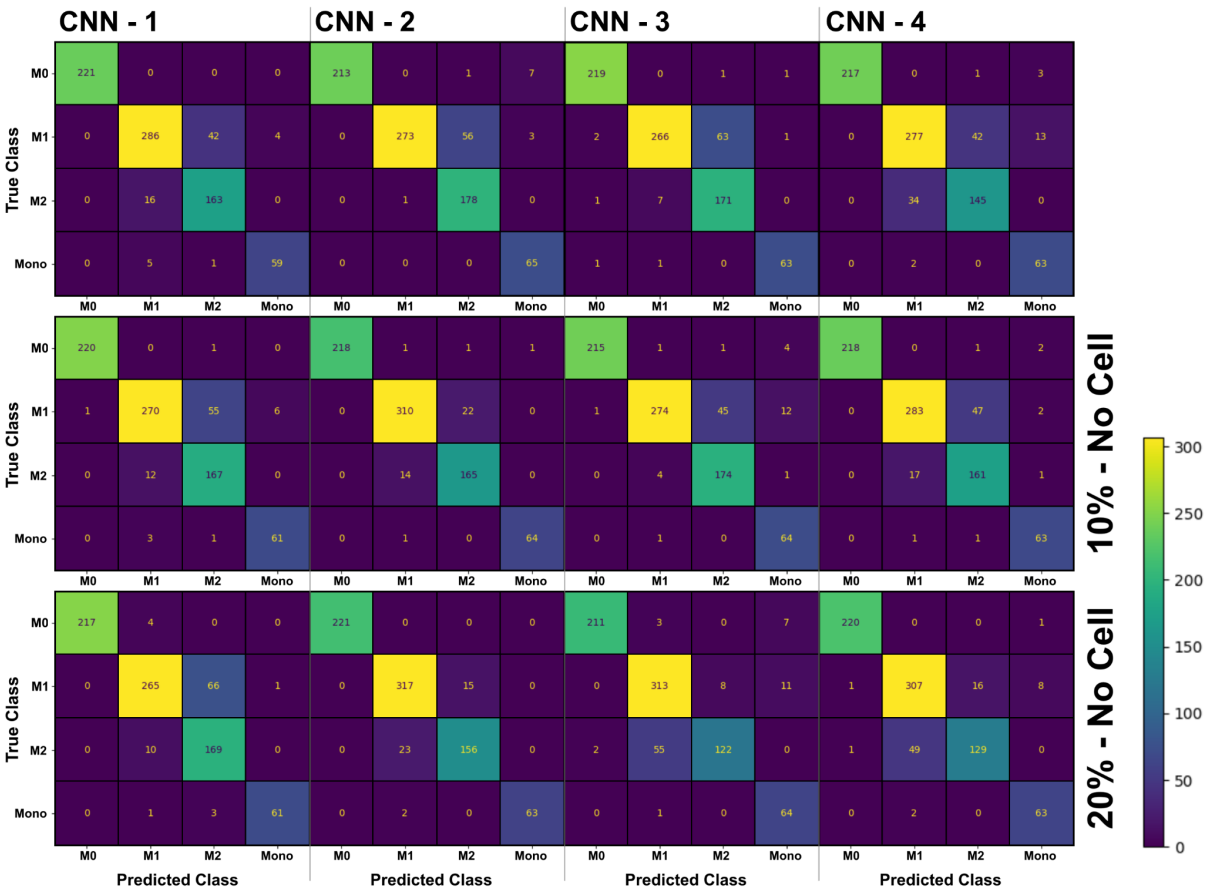

Fig. S4: Confusion matrix outcome for CNN models of Fig. S2 using an Epoch of 10 for 0%, 10% and 20% of no cell content (experimental sample errors) added to the investigated cell classes. The model predictions were tested for 221, 332, 179 and 65 cells for M0-, M1-, M2-macrophages and monocytes respectively (including the indicated no cell content). Results show a misclassification of 68, 68, 78 and 95 for 0% of no cell content; 79, 40, 70 and 72 for 10% of no cell content and 84, 40, 76 and 69 for 20% of no cell content for CNN – 1,2,3 and 4, respectively. This outcome highlights the performance of the CNN - 2 architecture for snapshot prediction.

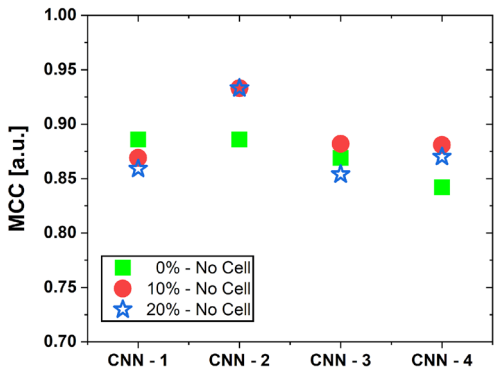

Fig. S5: Matthew Correlation Coefficient (MCC) calculated from the confusion matrix in Fig. S4. The higher the MCC score the better the model prediction.

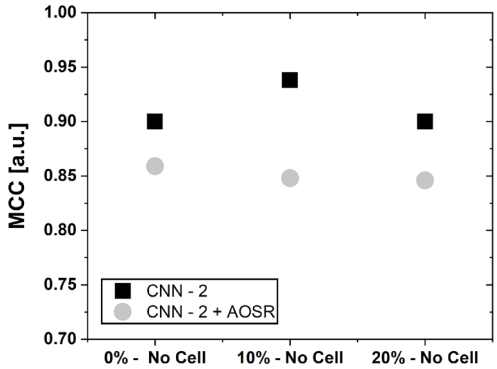

Fig. S6: Matthew Correlation Coefficient (MCC) calculated from the confusion matrix in Fig. 6 (CNN - 2) and Fig 8 (CNN – 2 + AOSR). The higher the MCC score the better the model prediction.

Table S2. Training accuracy and THP-1 detection rate of CNN - 2 architecture Fig. S3 (b) with alternating AOSR parameters β, Epoch 1 and 2. 10% of no cell content is highlighted in light grey, while 20% of no cell content is highlighted in dark grey.

β	**0.007**	**0.01**	**0.05**	**0.08**	**0.1**	**0.5**	**1**	**1.5**
Epoch 1 of AOSR	**2**	**2**	**2**	**2**	**2**	**2**	**2**	**2**
Epoch 2 of AOSR	**20**	**20**	**20**	**20**	**20**	**20**	**20**	**20**
10 Epoch - Training accuracy	96%	96%	90%	85%	92%	63%	48%	37%
10 Epoch - THP-1 detection	76%	80%	89%	94%	98%	100%	100%	100%
10 Epoch - Training accuracy	90%	90%	88%	88%	87%	69%	58%	51%
10 Epoch - THP-1 detection	18%	22%	78%	91%	94%	99%	100%	100%
10 Epoch - Training accuracy	85%	84%	82%	81%	80%	71%	57%	49%
10 Epoch - THP-1 detection	7%	11%	64%	81%	87%	98%	99%	99%
15 Epoch - Training accuracy	99%	99%	95%	92%	91%	69%	53%	43%
15 Epoch - THP-1 detection	79%	81%	90%	94%	95%	98%	99%	99%
15 Epoch - Training accuracy	92%	91%	89%	88%	87%	70%	57%	51%
15 Epoch - THP-1 detection	4%	6%	50%	67%	76%	95%	98%	99%
15 Epoch - Training accuracy	88%	88%	86%	85%	84%	66%	56%	48%
15 Epoch - THP-1 detection	25%	32%	57%	65%	74%	98%	100%	100%
20 Epoch - Training accuracy	99%	99%	94%	91%	89%	59%	40%	28%
20 Epoch - THP-1 detection	64%	67%	84%	88%	88%	95%	95%	97%
20 Epoch - Training accuracy	93%	92%	90%	88%	88%	65%	49%	38%
20 Epoch - THP-1 detection	26%	28%	74%	87%	93%	100%	100%	100%
20 Epoch - Training accuracy	89%	89%	86%	85%	84%	68%	54%	44%
20 Epoch - THP-1 detection	2%	3%	28%	47%	56%	98%	98%	98%

Epoch 1 of AOSR	**3**	**3**	**3**	**3**	**3**	**3**	**3**	**3**
Epoch 2 of AOSR	**30**	**30**	**30**	**30**	**30**	**30**	**30**	**30**
10 Epoch - Training accuracy	77%	96%	91%	88%	85%	63%	48%	38%
10 Epoch - THP-1 detection	0%	81%	91%	94%	95%	99%	100%	100%
10 Epoch - Training accuracy	90%	90%	88%	88%	87%	70%	59%	53%
10 Epoch - THP-1 detection	18%	23%	79%	91%	94%	99%	100%	100%
10 Epoch - Training accuracy	85%	84%	82%	81%	80%	72%	58%	53%
10 Epoch - THP-1 detection	7%	11%	66%	81%	87%	98%	99%	99%
15 Epoch - Training accuracy	99%	98%	95%	92%	91%	70%	54%	43%
15 Epoch - THP-1 detection	77%	82%	90%	93%	95%	98%	99%	99%
15 Epoch - Training accuracy	92%	91%	89%	88%	88%	71%	58%	51%
15 Epoch - THP-1 detection	4%	7%	51%	69%	77%	95%	97%	98%
15 Epoch - Training accuracy	88%	88%	86%	85%	84%	67%	56%	49%
15 Epoch - THP-1 detection	24%	30%	57%	68%	79%	98%	100%	100%
20 Epoch - Training accuracy	99%	99%	94%	91%	89%	60%	41%	29%
20 Epoch - THP-1 detection	62%	65%	84%	87%	88%	95%	95%	96%
20 Epoch - Training accuracy	93%	92%	90%	88%	87%	66%	51%	40%
20 Epoch - THP-1 detection	25%	28%	74%	89%	94%	100%	100%	100%
20 Epoch - Training accuracy	89%	89%	86%	85%	84%	68%	55%	45%
20 Epoch - THP-1 detection	3%	4%	30%	50%	57%	98%	97%	97%

Epoch 1 of AOSR	**4**	**4**	**4**	**4**	**4**	**4**	**4**	**4**
Epoch 2 of AOSR	**40**	**40**	**40**	**40**	**40**	**40**	**40**	**40**
10 Epoch - Training accuracy	97%	96%	91%	87%	85%	64%	49%	39%
10 Epoch - THP-1 detection	78%	83%	92%	94%	96%	100%	100%	100%
10 Epoch - Training accuracy	90%	90%	88%	87%	86%	70%	58%	50%
10 Epoch - THP-1 detection	21%	32%	85%	94%	96%	99%	100%	97%
10 Epoch - Training accuracy	85%	85%	82%	81%	80%	73%	60%	54%
10 Epoch - THP-1 detection	10%	14%	67%	81%	87%	98%	99%	99%
15 Epoch - Training accuracy	99%	98%	94%	91%	90%	68%	51%	41%
15 Epoch - THP-1 detection	79%	83%	91%	95%	96%	99%	99%	100%
15 Epoch - Training accuracy	91%	91%	89%	88%	87%	72%	58%	50%
15 Epoch - THP-1 detection	5%	9%	59%	75%	80%	97%	98%	99%
15 Epoch - Training accuracy	88%	88%	86%	85%	84%	68%	56%	49%
15 Epoch - THP-1 detection	24%	32%	57%	70%	78%	99%	100%	100%
20 Epoch - Training accuracy	99%	99%	93%	89%	87%	58%	38%	28%
20 Epoch - THP-1 detection	65%	70%	85%	90%	90%	96%	97%	98%
20 Epoch - Training accuracy	92%	92%	89%	88%	86%	65%	50%	39%
20 Epoch - THP-1 detection	29%	36%	85%	95%	96%	100%	100%	100%
20 Epoch - Training accuracy	89%	89%	86%	84%	83%	67%	53%	44%
20 Epoch - THP-1 detection	3%	5%	37%	56%	66%	99%	100%	100%

Epoch 1 of AOSR	**5**	**5**	**5**	**5**	**5**	**5**	**5**	**5**
Epoch 2 of AOSR	**50**	**50**	**50**	**50**	**50**	**50**	**50**	**50**
10 Epoch - Training accuracy	97%	88%	91%	87%	85%	63%	48%	39%
10 Epoch - THP-1 detection	79%	0%	92%	95%	96%	100%	100%	100%
10 Epoch - Training accuracy	90%	90%	88%	87%	86%	69%	56%	48%
10 Epoch - THP-1 detection	26%	36%	88%	95%	98%	100%	100%	100%
10 Epoch - Training accuracy	85%	85%	82%	81%	81%	73%	60%	53%
10 Epoch - THP-1 detection	13%	15%	67%	80%	85%	98%	99%	99%
15 Epoch - Training accuracy	98%	98%	94%	90%	89%	66%	50%	39%
15 Epoch - THP-1 detection	80%	81%	91%	95%	96%	99%	100%	100%
15 Epoch - Training accuracy	92%	91%	90%	89%	87%	72%	58%	49%
15 Epoch - THP-1 detection	5%	9%	61%	78%	83%	97%	98%	99%
15 Epoch - Training accuracy	88%	88%	86%	85%	84%	68%	56%	49%
15 Epoch - THP-1 detection	28%	35%	57%	72%	79%	99%	100%	100%
20 Epoch - Training accuracy	99%	98%	93%	89%	86%	57%	37%	26%
20 Epoch - THP-1 detection	68%	74%	87%	91%	92%	97%	98%	99%
20 Epoch - Training accuracy	92%	92%	89%	88%	86%	64%	48%	36%
20 Epoch - THP-1 detection	34%	40%	89%	96%	98%	100%	100%	100%
20 Epoch - Training accuracy	89%	89%	86%	84%	83%	67%	51%	43%
20 Epoch - THP-1 detection	3%	4%	40%	60%	69%	99%	100%	100%